

## Plasticity and microstructure of Zr-Cu-Al bulk metallic glasses

G. Kumar, T. Ohkubo, T. Mukai, and K. Hono

National Institute for Materials Science, 1-2-1 Sengen, Tsukuba 305-0047, Japan

Authors' copy for Scripta Materialia 57, 173-176 (2007), doi:10.1016/j.scriptamat.2007

### Abstract

A small variation in composition of  $(\text{Zr}_{50}\text{Cu}_{50})_{100-x}\text{Al}_x$  bulk metallic glasses (BMGs) results in a markedly different mechanical behavior. In contrary to the previous reports, no chemical or structural inhomogeneities were observed in the sample that exhibits a large plastic strain, indicating the plasticity of Zr-Cu-Al BMGs is not inherently related to their microstructural features. The shear bands in plastic  $\text{Zr}_{47.5}\text{Cu}_{47.5}\text{Al}_5$  show localized nanocrystallization whereas the macroscopically brittle  $\text{Zr}_{45}\text{Cu}_{45}\text{Al}_{10}$  shows no indications of nanocrystallization during deformation.

*Keywords:* Metallic glasses; Shear bands; Plastic deformation; Transmission sample preparation

The tendency of bulk metallic glasses (BMGs) to form localized shear bands [1-5] leads to rapid failures along a dominant shear band in tensile loading [1, 2]. However, in constrained loading geometries like bending [6] or uniaxial compression [7-9], the formation of multiple shear bands can be triggered resulting in a significant macroscopic plastic deformation. High plastic strain in some BMGs has been explained by medium-range-order [7], high Poisson's ratio [8], and structural or chemical inhomogeneities [9]. BMGs based on Zr-Cu system have received a significant attention because of their large compressive plastic strain [9,10, 12-14] and an unsettled issue of "strain hardening" as most of other BMGs exhibit softening caused by shear banding [2, 11, 15]. The large plasticity and strain hardening-type phenomena observed in  $\text{Zr}_{47.5}\text{Cu}_{47.5}\text{Al}_5$  BMG were attributed to chemical heterogeneities and Cu-rich nanocrystals [16]. However, Zr-Cu based BMGs are known to be particularly prone to surface artifacts in TEM specimens generated during thin foil preparation by electropolishing or ion milling [17, 18]. Such artifacts should not be confused as the microstructural features, which may mislead the structure-property relation in BMGs.

Recently, Lee *et al.* [10] and Chen *et al.* [13] have suggested deformation induced nanocrystallization as a possible reason for the enhanced plasticity of Zr-Cu based BMGs. They reported the formation of nanocrystallites all over the deformed Zr-Cu-Al BMGs, but this is unlikely as the plastic deformation of BMGs is localized in thin shear bands. In fact, Chen *et al.* showed that bending of  $\text{Zr}_{50}\text{Cu}_{50}$  melt-spun ribbons induces crystallization only in the shear bands.

The aim of this study is to investigate the correlation between the plasticity and microstructure in  $(\text{ZrCu})_{100-x}\text{Al}_x$  BMGs that show a wide range of compressive plastic strains despite a small variation in the compositions. The microstructure of the  $(\text{ZrCu})_{100-x}\text{Al}_x$  BMGs that show different amount of plastic strains has been characterized by TEM. In addition, three-dimensional atom probe (3DAP) was employed as a complementary characterization technique that yields information from the bulk of the specimen without getting any influence from surface artifacts.

Ingots of  $(\text{ZrCu})_{100-x}\text{Al}_x$  ( $x = 2, 5, 6, 8, 10$ ) were prepared by arc melting the pure elements under Ar atmosphere. The rod-shaped specimens of 2 mm diameter and approximately 60 mm in length were prepared by copper mold casting. Melt-spun ribbons of 50  $\mu\text{m}$  thickness were produced using a melt spinner at a wheel speed of 20  $\text{ms}^{-1}$ . The thermal properties were measured with a Perkin-Elmer Pyris 1 differential scanning calorimeter (DSC). Microstructure was characterized using a transmission electron microscopy (TEM) using a Philips CM200 TEM and a 3DAP. For TEM specimen preparation, it was noticed that decrease in ion milling energy is more effective to avoid the surface damage rather than lowering the specimen temperature. Thin foils were prepared by using a Gatan Precision Ion Polishing System (PIPS) starting at 2.8 keV and subsequently lowering the energy to 2 keV in steps. Additional low energy gentle milling at 200 eV was carried out prior to TEM observations. Atom probe specimens were prepared by focused-ion-beam (FIB). Room temperature uniaxial compression tests were conducted on cylindrical specimens of 2 mm diameter and 4 mm in length using an Instron machine at a constant strain rate of  $10^{-4} \text{ s}^{-1}$ . For TEM study of shear bands, the melt-spun ribbons were bent 180° and then straightened to approximately 15° in order to generate preferentially compressive or tensile stress. The bent ribbons were polished from one side in order to examine the shear bands generated in mainly compressive or tensile regions. For the bulk fractured specimens shear steps at surface were preserved, which enabled edge-on observation of shear bands.

The as-cast  $(\text{ZrCu})_{100-x}\text{Al}_x$  rods were examined by XRD which showed only broad halos for the all alloys (the data not shown). Figure 1 shows the DSC curves of as-cast  $(\text{ZrCu})_{100-x}\text{Al}_x$  rods recorded at a heating rate of 20 °C/min. The thermal behavior is manifested by a distinct endothermic event due to the glass transition ( $T_g$ ), followed by exothermic reaction corresponding to the crystallization ( $T_x$ ) of amorphous phase. The  $T_g$  and  $T_x$  increase monotonically with increasing Al content. All the specimens exhibit a single crystallization peak except for the  $\text{Zr}_{45}\text{Cu}_{45}\text{Al}_{10}$  that shows two-step crystallization event. The presence of the second exothermic peak for the  $\text{Zr}_{45}\text{Cu}_{45}\text{Al}_{10}$  sample is due to the formation of an additional crystalline phase. This is further supported by the decrease in the peak area of the first crystallization peak.

The room temperature compressive stress-strain curves of the as-cast specimens are shown in Fig. 2. The stress-strain curves are characteristic of a large elastic limit of about 0.2 for BMGs, followed by a yielding point and a serrated plastic deformation. There are several notable changes in the stress-strain curves with variation of Al content. Firstly, the increase in Al content more than 5 at.% reduces the plastic deformation significantly. No distinct plastic deformation is observed in the as-cast  $\text{Zr}_{45}\text{Cu}_{45}\text{Al}_{10}$  rod. In contrast, the as-cast  $\text{Zr}_{49}\text{Cu}_{49}\text{Al}_2$  and  $\text{Zr}_{47.5}\text{Cu}_{47.5}\text{Al}_5$  rods exhibit a plastic strain in the range of 0.05-0.07. Another distinct feature is that the compressive yield stress and elastic modulus (estimated from the slope of stress-strain

curves) show an abrupt increase with increasing the Al content beyond 5 at.%. The compressive yield stress for the  $Zr_{47.5}Cu_{47.5}Al_5$  rod is 1.7 GPa, which rise to 1.99 GPa for the  $Zr_{46}Cu_{46}Al_8$  rod suggesting a dramatic change in the local atomic structure.

The microstructures of as-cast  $Zr_{47.5}Cu_{47.5}Al_5$  and  $Zr_{45}Cu_{45}Al_{10}$  samples were examined in order to understand the possible reason for such a drastic change in mechanical behavior. Figure 3 compares the bright-field TEM images of as-cast  $Zr_{47.5}Cu_{47.5}Al_5$  and  $Zr_{45}Cu_{45}Al_{10}$  rods. The micrographs feature the presence of crystalline particles with an average size of 10 nm in an amorphous matrix. The corresponding selected area electron diffraction (SAED) patterns though show only a diffuse halo because of small size and volume fraction of the crystalline particles. The HRTEM results (not shown here) revealed that the crystalline particles are Cu-rich fcc phase with a lattice constant of 0.37 nm. These microstructural features are very similar to that observed in the previous work where the plasticity of  $Zr_{47.5}Cu_{47.5}Al_5$  BMG was correlated to presence of nanocrystals [16]. On the contrary, Fig. 3 clearly shows that the specimens with significantly different mechanical behavior display similar microstructural features. As mentioned earlier and also known from literature, an extra caution must be taken in interpreting the TEM results of Cu-containing BMGs because of their sensitivity to surface artifacts caused by thinning techniques. In order to verify whether or not the observed features represent the true microstructure the  $Zr_{47.5}Cu_{47.5}Al_5$  alloy was investigated in detail.

Figure 4a shows the bright-field TEM micrograph of the  $Zr_{47.5}Cu_{47.5}Al_5$  specimen that was ion milled at 2.8 keV. It can be clearly noticed that the crystalline contrast is nearly absent, indicating the strong effect of ion milling energy on the TEM specimen. To verify the TEM results further, 3DAP was used which yields information on the distribution of atoms within a needlelike specimen. Fig. 4b shows the 3DAP elemental maps of Zr, Cu and Al within analyzed volume of ( $13 \times 13 \times 70$  nm<sup>3</sup>) in the as-cast  $Zr_{47.5}Cu_{47.5}Al_5$  rod and the concentration frequency diagrams obtained from the data. The elemental maps show uniform distribution of the all alloying elements. The  $\chi^2$  test of the concentration distribution diagrams and the binomial distribution expected from homogeneous solid solution [19] confirmed that the as-cast  $Zr_{47.5}Cu_{47.5}Al_5$  sample was a homogeneous amorphous alloy. By comparing the length scales of the 3DAP atom maps and the TEM micrographs (Fig. 3a), the crystalline particles of as large as 10 nm should be readily detected with the 3DAP since the particles have been reported to be enriched with Cu [18].

In order to investigate the origin of the plastic strain in the  $(ZrCu)_{100-x}Al_x$  BMGs, the  $Zr_{47.5}Cu_{47.5}Al_5$  and  $Zr_{45}Cu_{45}Al_{10}$  alloys were chosen for shear band analysis because of their noticeably different mechanical behavior. Fig 5(a) shows a dark-field TEM micrograph of a shear band formed in the compressive region of bent  $Zr_{47.5}Cu_{47.5}Al_5$  ribbon. The location of the objective aperture is illustrated schematically in the inset. The image shows the precipitation of numerous nanocrystals along the shear band. As shown in the inset, the SAED pattern taken from the shear band exhibits spotty rings confirming the presence of crystallites in the sheared region. The crystallites are of 6-10 nm diameter. It should be noticed that no such crystallites are observed in the plastically-undefromed regions away from the shear band. Fig. 5(b) shows a dark-field TEM image of a typical compressive shear band in amorphous  $Zr_{45}Cu_{45}Al_{10}$  melt-spun ribbon, which also includes the corresponding SAED pattern. No crystalline phase is observed from the micrograph and the SAED pattern. As indicated in the inset, the objective

aperture was centered on the first halo. The shear band in Fig. 5b appears darker because of less thickness, as would be expected for a thin region where there is a less material to scatter the electrons. It has been reported that the contrast in the dark-field imaging of shear bands depends on the position of the objective aperture [20].

It is worth noting that there are significant differences between the compressive shear bands in the  $Zr_{47.5}Cu_{47.5}Al_5$  and  $Zr_{45}Cu_{45}Al_{10}$  melt-spun ribbons. For the  $Zr_{47.5}Cu_{47.5}Al_5$  ribbon, the shear bands are diffuse and contain abundant crystals. On the contrary, the shear bands in  $Zr_{45}Cu_{45}Al_{10}$  ribbon are much thinner and crystal-free. This difference in the structure of shear bands in melt-spun ribbons is expected to have significant implications for the mechanical behavior of bulk counterparts, e.g., the  $Zr_{47.5}Cu_{47.5}Al_5$  BMG shows large plastic strain whereas the  $Zr_{45}Cu_{45}Al_{10}$  BMG is macroscopically brittle (Fig. 2). The stress state in the bulk specimens during compression tests is different than that of ribbons during bending. The difference in the stress state for the bulk specimens and ribbons may affect the deformation-induced structural changes. Figure 6(a) shows a dark-field TEM image of shear bands in a cylindrical  $Zr_{47.5}Cu_{47.5}Al_5$  BMG after compression test. Three shear bands can be clearly identified from the surface steps (marked with arrows). The formation of crystals in shear bands is evident from the image and the corresponding SAED pattern shown in the inset, which also indicates the position of objective aperture. The crystals are observed only in the shear bands and no crystals can be seen in the plastically-undeformed region. The crystals are as large as 30 nm in diameter, which is significantly larger compared to that of melt-spun ribbon (Fig. 6a). The shear bands were also identified with an optical microscope prior to the TEM observations. Furthermore, the shear bands and cracks can be distinguished from the continuity of the specimen at the edge. The shear bands are thinner at the edge and become thicker farther away beyond the crystals. This is most likely caused by the formation of crystals which hinder the plastic flow along the shear bands.

To distinguish the effect of plastic deformation and ion milling on the formation of nanocrystals in shear bands, the tensile region of bent ribbons was analyzed. Fig. 7b shows a dark-field TEM image of a typical shear band in tensile region of melt-spun  $Zr_{47.5}Cu_{47.5}Al_5$  ribbon. No crystallization in the shear band is observed in tensile region. The micrograph clearly shows that the shear band is not preferentially crystallized by ion milling. Therefore, it can be unambiguously stated that the difference in the structure of shear bands in compressive and tensile regions of melt-spun  $Zr_{47.5}Cu_{47.5}Al_5$  ribbons is related to the stress state and the nanocrystallization at the shear bands is not caused by TEM specimen preparation.

This study has unambiguously shown that the plastic deformation in as-cast  $(ZrCu)_{100-x}Al_x$  BMGs is strongly sensitive to the composition despite their amorphous structure. The TEM micrographs show crystalline features when the specimens are thinned by ion milling at energy higher than 3 keV. Similar microstructural features have been previously reported for Zr-Cu based BMGs where the plasticity was correlated to these features [16]. However, our comprehensive TEM analysis corroborated with the 3DAP results show that the specimens are homogeneous amorphous. The bulk specimens with different plastic strain as well as the melt-spun ribbons show similar microstructural features when the TEM samples are prepared under the same conditions. This clearly suggests that the plasticity of amorphous Zr-Cu-Al alloys is not inherently related to the frequently observed microstructural features in the TEM images. The formation of real microstructural inhomogeneities would certainly affect the mechanical

properties, however, even monolithic BMGs like Zr-Ta-Ni-Cu-Al and Pt-Cu-Ni-P can show large plasticity [7, 8].

The strong compositional dependence of plasticity of Zr-Cu-Al BMGs can be convincingly explained by considering the change in competing crystalline phases and the activation energy for crystallization. According to a recent work by Wang *et al.* in Zr-Cu-Al system, the primary phase would change from  $Zr_{50}Cu_{50}$  to ternary  $Zr_{38}Cu_{36}Al_{26}$  with increasing Al more than 6 at.% along  $(ZrCu)_{100-x}Al_x$  compositions [21]. This change in primary crystalline phase may impede deformation-driven phase transformation in the compositions where long-range diffusion is needed for crystallization. This can also explain why no plasticity was observed in previously studied amorphous Zr-Cu-Al compositions [22]. In binary  $Zr_{50}Cu_{50}$  the transformation from amorphous structure to monoclinic  $Zr_{50}Cu_{50}$  does not require long-range diffusion. Additionally, the tendency to form crystals during deformation and the resultant plastic strain in Zr-Cu-Al BMGs can be understood from the activation energy for crystallization. The activation energy for crystallization estimated by Kissinger's method is 330 and 367 kJ/mol for amorphous  $Zr_{47.5}Cu_{47.5}Al_5$  and  $Zr_{45}Cu_{45}Al_{10}$  ribbons, respectively. The increase in activation energy is due to change in the primary crystallization product from  $Zr_{50}Cu_{50}$  to  $Zr_{38}Cu_{36}Al_{26}$  with increasing Al content. It is unlikely that the temperature rise at shear bands in  $Zr_{47.5}Cu_{47.5}Al_5$  and  $Zr_{45}Cu_{45}Al_{10}$  amorphous alloys will be significantly different. Therefore, during plastic deformation amorphous  $Zr_{47.5}Cu_{47.5}Al_5$  alloy is more susceptible to crystallization because of its lower activation energy compared to amorphous  $Zr_{45}Cu_{45}Al_{10}$  alloy. These assertions are supported by the present TEM investigations, which reveal crystals in shear bands of  $Zr_{47.5}Cu_{47.5}Al_5$  ribbon but no crystals are detected in shear bands of  $Zr_{45}Cu_{45}Al_{10}$  ribbon. Absence of nanocrystals in the shear bands of tensile region rules out the possibility of preferential ion milling damage occurring at shear bands. Several studies have indicated that the Poisson's ratio in Zr-Cu-Al BMGs remains in the range of 0.36-0.37 for a wide range of compositions [23-25]. Therefore, the drastic change in the mechanical behavior observed in  $(ZrCu)_{100-x}Al_x$  BMGs cannot be explained by the change in the Poisson's ratio. All these observations unanimously suggest that the plasticity of Zr-Cu based BMGs is related to their tendency to form crystallites during deformation. To our knowledge, there is only one study [26] in addition to the present work, which comprehensively showed that nanocrystallization of metallic glasses at shear bands occurs preferentially in the compressive regions.

In summary, a strong composition dependence of plastic strain in amorphous  $(ZrCu)_{100-x}Al_x$  alloys has been observed, which can be explained by structural changes in the shear bands. The alloy compositions with primary phase  $Zr_{50}Cu_{50}$  exhibit large plastic strain facilitated by deformation-induced nanocrystallization in the shear bands. The alloys with primary phase other than  $Zr_{50}Cu_{50}$  do not form crystals in the shear bands and consequently are macroscopically brittle. The difference in crystallization behavior during deformation stems from the change in the primary crystalline phase and the activation energy for crystallization. This work has clearly demonstrated that the heterogeneities observed in Zr-Cu-Al BMGs are merely caused by TEM sample preparation. It is concluded that the presence of phase separation or quenched-in crystallites is not an essential prerequisite for the large plasticity of Zr-Cu and Zr-Cu-Al BMGs.

We thank Dr. K. Mondal and Y. Chen for useful discussions. The work was supported by a Grant in Aid of the Ministry of Education, Sports, Culture, Science and Technology, Priority Area on “Materials Science of Bulk Metallic Glasses”.

## References

- [1] C. A. Pampillo, *J. Mater. Sci.* **10** (1975) 1194.
- [2] T. Masumoto, R. Maddin, *Mater. Sci. Eng. A* **19** (1975) 1.
- [3] F. Spaepen, *Acta Metall* **25** (1975) 407.
- [4] A. S. Argon, *Acta Metall* **27** (1979) 47.
- [5] P. E. Donovan, *Acta Mater* **37** (1989) 445.
- [6] R. D. Conner, Y. Li, W. D. Nix, W. L. Johnson, *Acta Mater.* **52** (2004) 2429.
- [7] L. Q. Xing, Y. Li, K. T. Ramesh, J. Li, T. C. Hufnagel, *Phys. Rev. B* **64** (2001) R180201.
- [8] J. Schroers, W. L. Johnson, *Phys. Rev. Lett.* **93** (2004) 255506.
- [9] J. Das, M. B. Tang, K. B. Kim, R. Theissmann, F. Baier, W. H. Wang, J. Eckert, *Phys. Rev. Lett.* **94** (2005) 205501.
- [10] S. W. Lee, M.Y. Huh, E. Fleury, J.C. Lee, *Acta Mater.* **54** (2006) 349.
- [11] Y. Zhang, W. H. Wang, A. L. Greer, *Nature Mater.* **5** (2006) 857.
- [12] Y. F. Sun, B. C. Wei, Y. R. Wang, W. H. Li, T. L. Cheung, C. H. Shek, *Appl. Phys. Lett.* **87** (2005) 051905.
- [13] M. Chen, A. Inoue, W. Zhang, T. Sakurai, *Phys. Rev. Lett.* **96** (2006) 245502.
- [14] K. Hajlaoui, A. R. Yavari, B. Doisneau, A. LeMoulec, W. J. Botta, G. Vaughan, A. L. Greer, A. Inoue, W. Zhang, A. Kvick, *Scripta Mater.* **54** (2006) 1829.
- [15] H. Bei, S. Xie, E. P. George, *Phys. Rev. Lett.* **96** (2006) 105503.
- [16] K. B. Kim, J. Das, F. Baier, M. B. Tang, W. H. Wang, J. Eckert, *Appl. Phys. Lett.* **88** (2006) 051911.
- [17] B. B. Sun, Y. B. Wang, J. Wen, H. Yang, M. L. Sui, J. Q. Wang, E. Ma, *Scripta Mater.* **53** (2005) 805.
- [18] D. Nagahama, T. Ohkubo, T. Mukai, K. Hono, *Mater. Trans.* **46** (2005) 1264.
- [19] M. K. Miller, *Atom Probe Tomography: Analysis at the Atomic Level*, Kluwer Academics, New York, 2000.
- [20] P.E. Donovan, W. M. Stobbs, *Acta Metall* **29** (1981) 1419.
- [21] D. Wang, H. Tan, Y. Li, *Acta Mater.* **53** (2005) 2969.
- [22] A. Inoue, W. Zhang, *Mater Trans.* **43** (2002) 2921.
- [23] W. H. Wang, *J. Appl. Phys.* **99** (2006) 093506.
- [24] G. J. Fan, M. Freels, H. Choo, P. K. Liaw, J. J. Z. Li, W. K. Rhim, W. L. Johnson, P. Yu, W. H. Wang, *Appl. Phys. Lett.* **89** (2006) 241917
- [25] Y. Yokoyama, T. Yamasaki, P. K. Liaw, R. A. Buchanan, A. Inoue, *Mater. Sci. Eng. A* (2006) in press.
- [26] W. H. Jiang, M. Atzmon, *Acta Mater.* **51** (2003) 4095.

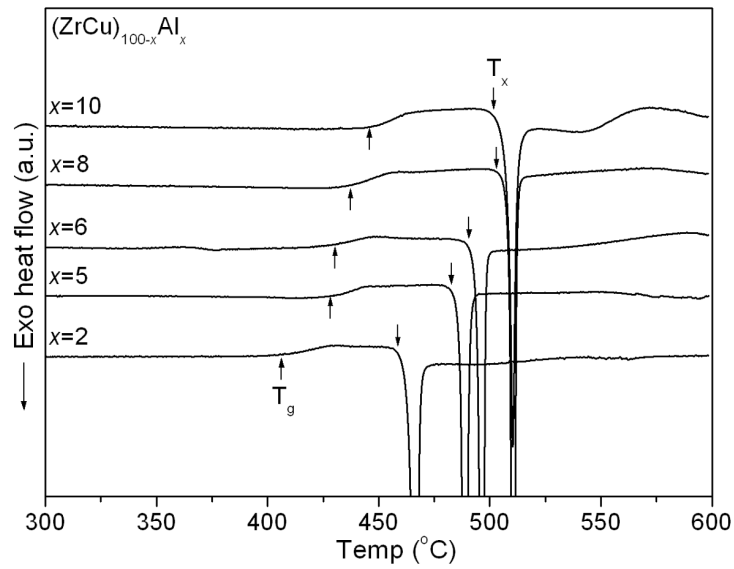


**Fig. 1:** DSC curves of as-cast  $(\text{ZrCu})_{100-x}\text{Al}_x$  rods measured at a heating rate of  $20\text{ }^\circ\text{C}/\text{min}$ . The onset of  $T_g$  and  $T_x$  are indicated by arrows.

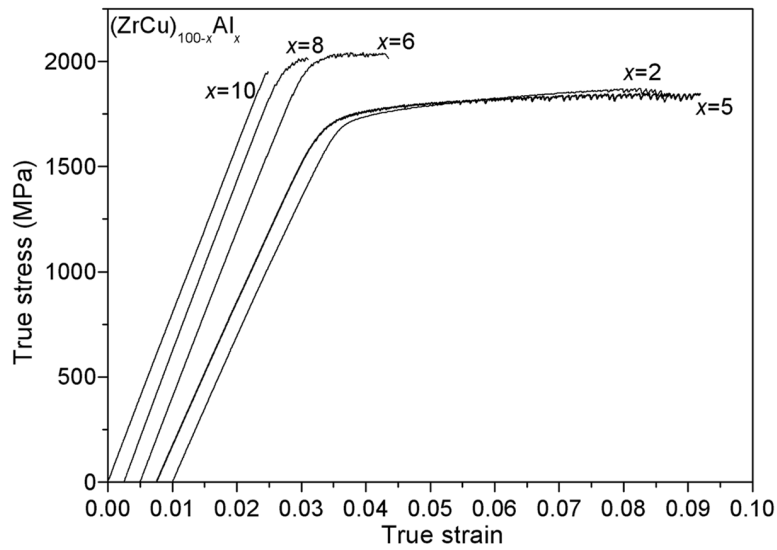


**Fig. 2:** Compressive stress-strain curves of as-cast  $(\text{ZrCu})_{100-x}\text{Al}_x$  rods at a strain rate of  $10^{-4}\text{ s}^{-1}$ .

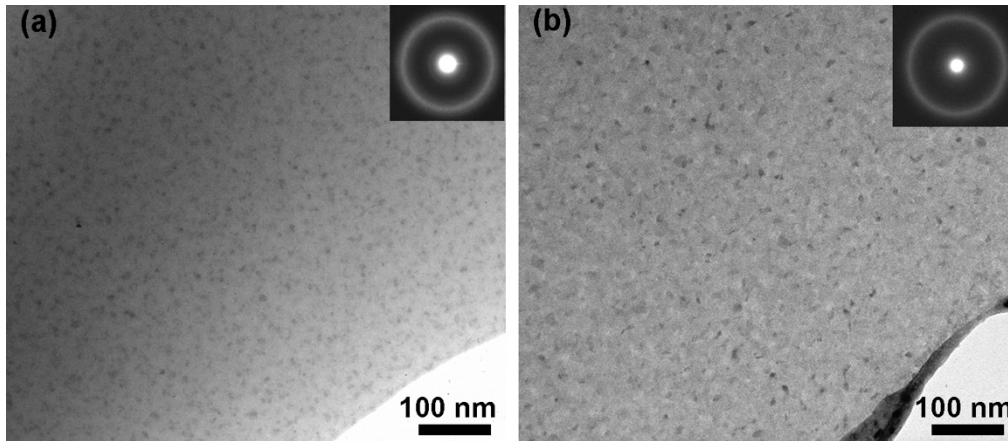


**Fig. 3:** Bright-field TEM micrographs and the corresponding SAED patterns of as-cast (a)  $Zr_{47.5}Cu_{47.5}Al_5$  and (b)  $Zr_{45}Cu_{45}Al_{10}$  rods. The TEM specimens were prepared at 4 keV.

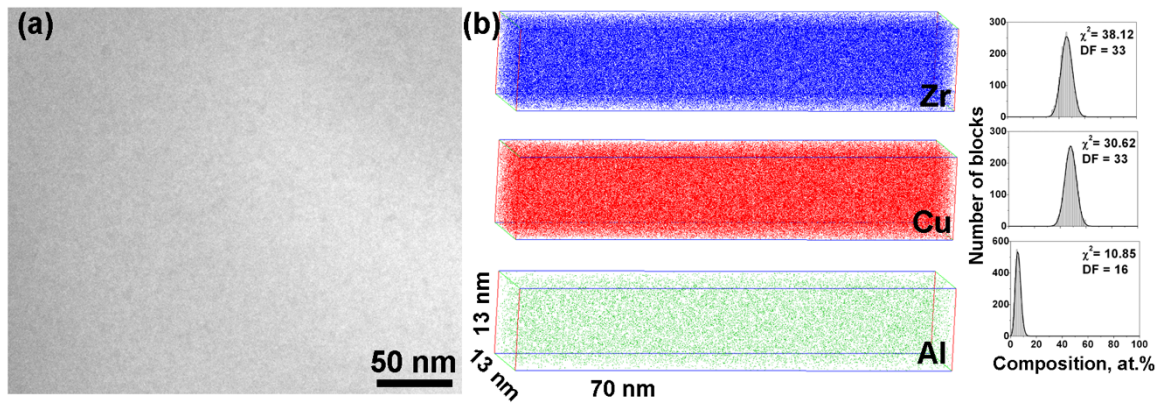


**Fig. 4:** (a) Bright-field TEM micrograph after preparing the TEM specimens at 2.8 keV and (b) 3DAP elemental mappings and frequency distribution diagrams of Zr, Cu and Al in a selected volume of  $(13 \times 13 \times 70 \text{ nm}^3)$  from the as-cast  $Zr_{47.5}Cu_{47.5}Al_5$  rod.  $\chi^2$  and degree of freedom (DF) are shown in the graphs.

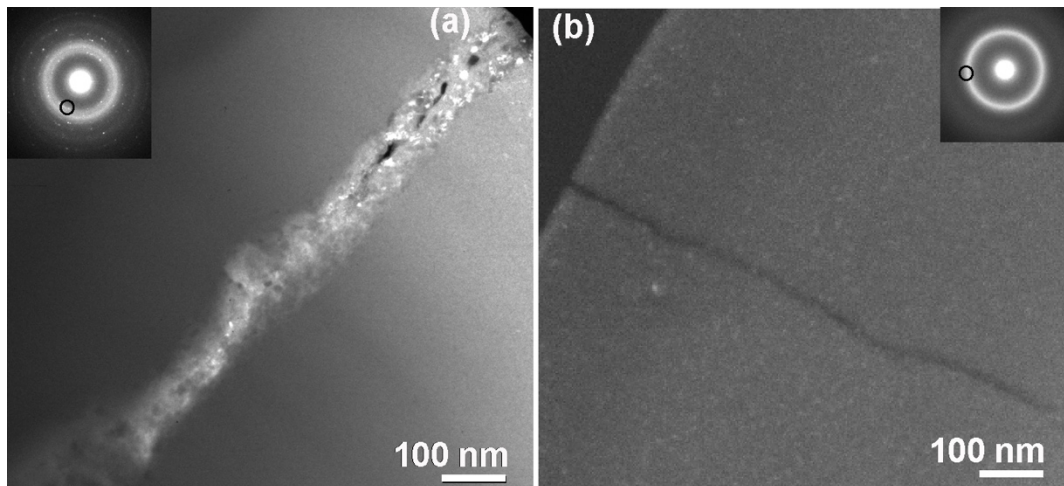


**Fig. 5:** Dark-field TEM images of a shear band in compressive region of melt-spun (a)  $Zr_{47.5}Cu_{47.5}Al_5$  and (b)  $Zr_{45}Cu_{45}Al_{10}$  ribbons. Insets are the SAED patterns taken from the sheared regions. The position of the objective aperture is illustrated schematically.

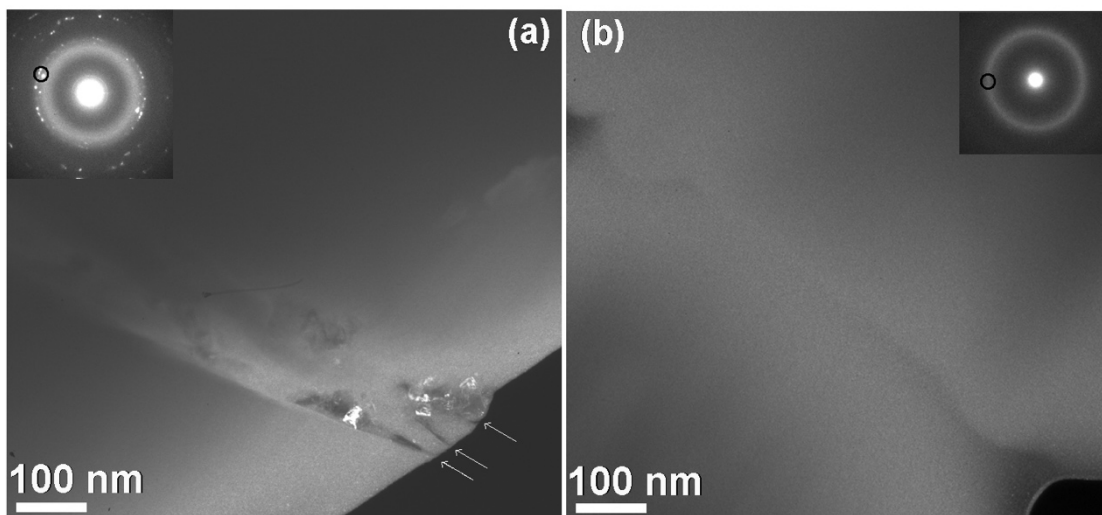


**Fig. 6:** Dark-field TEM images of a shear band in (a) bulk  $Zr_{47.5}Cu_{47.5}Al_5$  amorphous alloy after compression test compressive region and (b) tensile region of melt-spun  $Zr_{47.5}Cu_{47.5}Al_5$  ribbon. Insets are the SAED patterns taken from the sheared regions.